C. R. Physique 13 (2012) 470–479

Contents lists available at SciVerse ScienceDirect

Comptes Rendus Physique

www.sciencedirect.com

Advances in nano-electromechanical systems

Putting mechanics into circuit quantum electrodynamics

La mécanique en électrodynamique quantique des circuits

Nicolas Didier *, Rosario Fazio

Scuola Normale Superiore, NEST and Istituto NanoScienze-CNR, 56126 Pisa, Italy

ARTICLE INFO

Article history:
Available online 28 March 2012

Keywords:
Nano-electromechanical systems
Superconducting nanocircuits
Microwave cavity
Quantum bit
Entanglement
Quantum master equation

Mots-clés :
Nano-systèmes électro-mécaniques
Nano-circuits supraconducteurs
Cavité micro-onde
Bit quantique
Intrication
Équation maîtresse quantique

ABSTRACT

We review the use of mechanical oscillators in circuit quantum electrodynamics. The capacitive coupling of nano-electromechanical systems with quantum bits and superconducting microwave resonators gives rise to a rich quantum physics involving electrons, photons and phonons. We focus in particular on the linear coupling between a mechanical oscillator and a microwave resonator and present the quantum dynamics that stems from the phonotonic Josephson junction. The microwave cavity turns out to be a powerful device to detect quantum phonon states and manipulate entangled states between phonons and photons.

RÉSUMÉ

Nous étudions l'utilisation des oscillateurs mécaniques dans le domaine de l'électrodynamique quantique en circuit. Le couplage capacitif des nano-systèmes électro-mécaniques avec des bits quantiques et des résonateurs supraconducteurs micro-ondes donne lieu à une physique riche mettant en jeu les électrons, les photons et les phonons. Nous nous intéressons en particulier au couplage linéaire entre un oscillateur mécanique et un résonateur micro-onde et nous présentons la physique de la jonction phonotonique. La cavité micro-onde s'avère être un dispositif efficace pour détecter des états quantiques de phonons et manipuler des états intriqués entre phonons et photons.

1. Introduction

Quantum effects in nano-electromechanical systems (NEMS) [1,2] are of great interest and intensively studied for a number of good reasons. Nanostructures, embedding mechanical oscillators, in which electron transport is coupled to the motion of the oscillator will form the core of new generations of high performance sensing devices. In addition to their impact in applied science, the experimental realization of nanomechanical oscillators widens the possibility to explore the fundaments of quantum mechanics and its crossover to the classical world [3]. The observation of a truly quantum dynamical behavior in a system containing millions of atoms would help in pushing upward the very elusive crossover between micro and macro which, before the development of nanoscience, was confined to be close to the molecular level. Since many years the Holy Grail in NEMS was to bring a mechanical oscillator in a state of zero-point motion. Several theoretical proposals designed

* Corresponding author.
E-mail addresses: nicolas.didier@sns.it (N. Didier), fazio@sns.it (R. Fazio).

1631-0705/$ – see front matter
doi:10.1016/j.crhy.2012.01.001

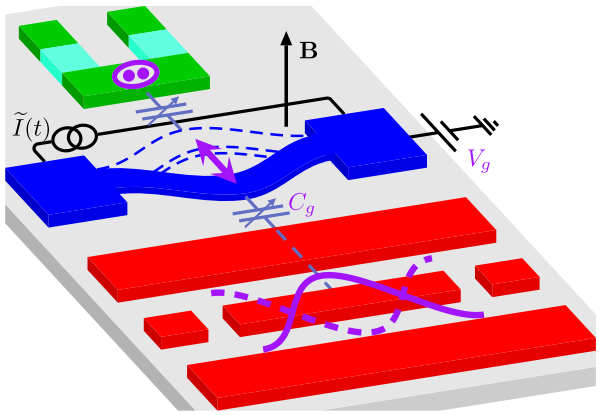

Fig. 1. Scheme of the phonotonic Josephson junction. A mechanical oscillator is capacitively coupled to an artificial atom and a superconducting microwave resonator. The NEMS is driven with an oscillating Laplace force.

ingenuous scheme of cooling [4] and over the years a series of important experiments [5] progressively reduced the number of quanta of excitations. The ground state was reached only very recently in three experimental groups with different NEMS and cooling techniques. First, a high frequency (in the GHz range) mechanical oscillator was coupled to a superconducting quantum bit (qubit) to detect its quantum properties [6]. Second, a low frequency (in the MHz range) mechanical oscillator was cooled down with sideband cooling using a superconducting microwave resonator (SMR) [7]. Third, laser cooling was used on an optomechanical cavity of a photonic crystal [8]. The realization and the manipulation of mechanical resonators at the quantum level makes these systems appealing also for quantum information processing where they can be employed as memory elements [9–11] or as a quantum bus [9,10,12].

As discussed in numerous theoretical papers and verified in a number of beautiful experiments (see, for example, the review by Clarke and Wilhem [13]) superconducting nanocircuits are excellent candidates to implement quantum information protocols in solid state architectures. Great attention has been devoted in the recent literature to the coupling between mechanical resonators and superconducting nanocircuits in several different regimes. The coupling to a Cooper pair box has been considered, for example, in Refs. [14–19], while the opposite regime with phase qubits has been considered in Refs. [9, 10,20,21]. Recently the dispersive coupling of a NEMS to a Cooper-pair box has been realized [22]. Coupling nanomechanical oscillators to SQUIDs has been also intensively investigated [23–27]. The high sensitivity of SQUIDs to tiny changes in the magnetic flux allows to detect the tiny motion of the resonator. A crucial experiment in this direction has been the detection of the thermal motion of a mechanical resonator in the classical regime [28].

Typical frequencies involved in the dynamics of the superconducting nanocircuits are in the GHz range, on the other side the frequencies associated to the mechanical motion can be much lower if one aims at large quality factors. Entering the quantum regime requires frequencies of the same order of magnitude (as in the experiment by Cleland [6]), however at the moment these GHz oscillators are plagued by very low quality factors. A full quantum dynamical manipulation will certainly benefit from having the two systems (the oscillator and the qubit) close to resonance with the damping effects reduced as much as possible.

In the present contribution we concentrate on the coupling between two kinds of oscillator, a mechanical resonator coupled to an SMR. The reasons for looking at this situation are many and of different nature. The amazing progresses in circuit quantum electrodynamics (circuit-QED) [29] have shown that these solid state realizations of QED systems have enormous potential in quantum information processing. One can therefore imagine that by engineering a suitable coupling to mechanical resonators one can use the level of manipulation achieved in circuit-QED to control the quantum evolution of the mechanical system. Superconducting cavities may be of importance also for the detection, at the moment we do not know direct means to reveal the quantum state of a mechanical system. Finally an efficient interface to photons is important for quantum information transfer. By itself a coupling between phonons in the resonators and photons in the cavity leads to a linear system. A much richer situation is achieved if nonlinearities are introduced in the devices. A controllable way to do this is to couple the mechanical resonator to a charge qubit.

The aim of this article is to review the properties of mechanical resonators coupled to SMRs in the presence of nonlinearities induced by the presence of a charge qubit. We will give some details in the derivation of the model appropriate to describe the system. We will also provide few examples of the flexibility of the device which can be used as a detection or preparation of quantum states of the mechanical oscillators. These examples are mainly based on our work [30,31] and are not intended by far to be a complete overview of the field.

The article is organized as follows: we explain first how to couple a NEMS to a qubit and an SMR to obtain the phonotonic Josephson junction drawn in Fig. 1. Then we show how to use this system to detect the phonon blockade phenomenon. Finally we present how to synthesize hybrid Bell states between photons and phonons.

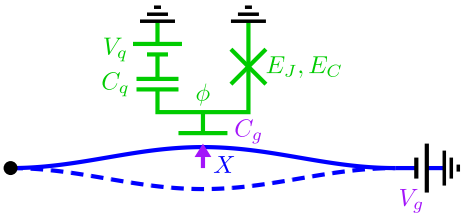

Fig. 2. Coupling to a qubit.

2. Interaction between phonons, electrons and photons

In circuit-QED a NEMS can be approached to different electrical elements, such as qubits and SMRs, to create a coupling capacitance that depends on the displacement X of the nanobeam from the position at rest. The amplitude being close to the zero point fluctuations X_{zpf}, the first order correction in the displacement is enough to describe the behavior of the capacitance. We define the reduced displacement $x = X/X_{\text{zpf}}$, which can be also written as $x = a + a^\dagger$ in terms of the canonical bosonic ladder operators a and $a^\dagger$ satisfying the commutation rule $[a, a^\dagger] = 1$. The Hamiltonian of the free NEMS of frequency ω_m is then $\hbar\omega_m(a^\dagger a + 1/2)$. If we note d the distance when $X = 0$, the corresponding capacitance $C^{(0)}$ is defined from the surface of the electrodes S according to $C^{(0)} = \epsilon_m S/d$, where ϵ_m is the permittivity of the medium. Then the capacitance at the distance $d - X$ reads $C(X) = C^{(0)}(1 - X/d) \simeq C^{(0)} + C^{(1)}x$ with $C^{(1)} = \frac{X_{\text{zpf}}}{d}C^{(0)}$. To generate a tunable coupling between the NEMS and electric elements we add a gate voltage V_g on the NEMS, see Figs. 2 and 3. In the following subsections we calculate first the coupling Hamiltonian between a NEMS and a qubit, then the coupling with an SMR, next the Lindbladian due to the coupling with the environment and finally we show how the coupling to an external circuit can generate a driving on the NEMS.

2.1. Coupling to a Cooper pair box

We consider a Cooper pair box close to a NEMS to create a capacitive coupling between the Cooper pairs on the island and the displacement of the nanobeam. The electric scheme is depicted in Fig. 2. The Cooper pair box is composed of a Josephson junction and a gate capacitance C_q, creating an island on which the tunneling of the Cooper pairs can be controlled. The Josephson junction is characterized by its Josephson energy E_J and its charging energy $E_C = (2e)^2/2C_J$. A gate voltage V_q is applied on the island and another one V_g on the NEMS. When only zero or one Cooper pair can sit on the island, the Cooper pair box constitutes a charge qubit.

The Lagrangian $\mathcal{L}$ is derived from the Kirchhoff laws

$$\mathcal{L} = \frac{C_q}{2}(\dot\phi - V_q)^2 + \frac{C_g}{2}(\dot\phi - V_g)^2 + \frac{C_J}{2}\dot\phi^2 + E_J\cos\phi \tag{1}$$

where ϕ is the phase on the island. The corresponding Hamiltonian, depending on the conjugate charge $Q = \partial\mathcal{L}/\partial\dot\phi$ and at first order in the displacement X, reads

$$\mathcal{H} = \frac{(Q+Q_0)^2}{2C_\Sigma} - \frac{C_g^{(1)}}{2C_\Sigma^2}(Q+Q_0)^2X + \frac{C_g^{(1)}V_g}{C_\Sigma}(Q+Q_0)X - E_J\cos\phi \tag{2}$$

where $C_\Sigma = C_J + C_q + C_g$ is the total capacitance and $Q_0 = C_qV_q + C_gV_g$ is the gate charge. From the commutation rule $[Q, \phi] = i2e$, the charge and the cosine of the phase can be expressed in the charge states $|n\rangle$ [32]: $Q = 2e\sum_n n|n\rangle\langle n|$ and $\cos\phi = \frac{1}{2}\sum_n |n\rangle\langle n+1| + |n+1\rangle\langle n|$. We now consider the Cooper pair box as a charge qubit, where only the charge states $|0\rangle$ and $|1\rangle$ are involved in the dynamics. Then

$$\mathcal{H} = \frac{1}{2}E_\Sigma(1+2n_0)s_z - \frac{1}{2}E_Js_x - \frac{C_g^{(1)}}{2C_\Sigma}E_\Sigma(1+2n_0)s_zx + n_gE_\Sigma s_zx \tag{3}$$

with the reduced gate charges $n_g = C_g^{(1)}V_g/2e$ and $n_0 = Q_0/2e$, the charging energy $E_\Sigma = (2e)^2/2C_\Sigma$, and the operators $s_z = |1\rangle\langle 1| - |0\rangle\langle 0|$ and $s_x = |1\rangle\langle 0| + |0\rangle\langle 1|$.

The Hamiltonian of the qubit can be diagonalized for $x = 0$. The eigenbasis σ_z, σ_x corresponds to a rotation of an angle θ defined by $\tan 2\theta = -E_J/E_\Sigma(1+2n_0)$. We are interesting in the quantum regime $n_0 = -1/2$ ($\theta = \pi/4$) where the eigenstates $|e\rangle$ and $|g\rangle$ are the symmetric superposition of the states $|0\rangle$ and $|1\rangle$, $\sigma_x = s_z$ and $\sigma_z = -s_x$. The coupling terms are of the type $\sigma_x x = (\sigma_+ + \sigma_-)(a + a^\dagger)$ with a strength $g_q = n_gE_\Sigma/\hbar$, $\sigma_+ = |e\rangle\langle g|$ and $\sigma_- = \sigma_+^\dagger$ are the ladder operators of the qubit. The coupling strength is usually much smaller than the qubit and mechanical energies, and a rotating wave approximation can be safely applied, leading to the well-known Jaynes–Cummings term $a\sigma_+ + a^\dagger\sigma_-$. Including the Hamiltonian of the mechanical oscillator, the Hamiltonian becomes

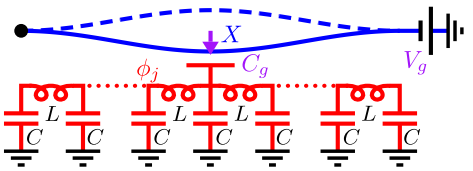

Fig. 3. Coupling to a superconducting microwave resonator.

$$\mathcal{H} = \hbar\omega_m a^\dagger a + \frac{1}{2}\hbar\omega_q \sigma_z + \hbar g_q\left(a^\dagger\sigma_- + a\sigma_+\right) \tag{4}$$

The main effect of the qubit on the mechanical resonator is to induce a nonlinearity in the spectrum. Indeed, each phonon state $|n\rangle$ is associated with two states of the qubit separated by an energy $2\hbar g_q\sqrt{n}$. This nonlinearity can be seen as an effective interaction between phonons, proportional to the phonon number squared. The effective interaction is of the Kerr type $H_{\text{Kerr}} = \hbar\kappa a^\dagger a^\dagger aa$, written is the normal order form.

To calculate the Kerr interaction it is necessary to average out the qubit. To proceed it is more convenient to use the states of the qubit dressed by a microwave excitation. A microwave sent on the qubit at the frequency ω_{mw} acts on the charge $Q \propto s_z = \sigma_x$, with the coupling proportional to $\sigma_x \cos\omega_{\text{mw}} t$. When the microwave frequency is close to the resonance, the rotating wave approximation can be used to simplify the Hamiltonian to

$$\mathcal{H}_{\text{mw}} = \hbar\Omega\left[\sigma_+ e^{-i\omega_{\text{mw}}t} + \sigma_- e^{i\omega_{\text{mw}}t}\right] \tag{5}$$

where Ω is the so-called Rabi frequency. Then going first in the frame rotating at ω_{mw} in resonance with the qubit $\omega_{\text{mw}} = \omega_q$ and then back to the charge basis yields

$$\mathcal{H} = \hbar\omega_m a^\dagger a + \frac{1}{2}\hbar\Omega s_z + \frac{1}{2}\hbar g_q\left[\left(a^\dagger e^{-i\omega_q t} + a e^{i\omega_q t}\right)s_z + \left(a^\dagger e^{-i\omega_q t} - a e^{i\omega_q t}\right)(s_+ - s_-)\right] \tag{6}$$

The last term is treated as a perturbation and its effect on the free Hamiltonian is evaluated at forth order. The main contribution is

$$\mathcal{H} = \hbar\omega_m a^\dagger a + \frac{1}{2}\hbar\Omega s_z + \left[-\frac{\hbar\Omega(g_q/2)^2}{2\Delta^2}a^\dagger a + \hbar\kappa a^\dagger a^\dagger aa\right]s_z \tag{7}$$

where $\Delta = \Omega - \omega_m$ is the detuning between the qubit and the NEMS, and the Kerr nonlinearity strength is

$$\kappa = \frac{(g_q/2)^4}{\Omega\Delta^2} \tag{8}$$

The main corrections do not act as a driving on the qubit, which then stays in the ground state. The adiabatic elimination of the qubit just consists of projecting on the ground state. Finally, the Hamiltonian of a NEMS coupled to a dressed qubit after adiabatic elimination of the latter reads

$$\mathcal{H} = \hbar\tilde{\omega}_m a^\dagger a - \hbar\kappa a^\dagger a^\dagger aa \tag{9}$$

with a slightly renormalized frequency $\tilde{\omega}_m = \omega_m + \Omega(g_q/2)^2/2\Delta^2$.

2.2. Coupling to a superconducting microwave resonator

The coupling between an SMR and a mechanical oscillator comes from the position dependent capacitance between the nanobeam and the signal line, $C_g(X) \simeq C_g^{(0)} + C_g^{(1)}X$. The electric scheme is presented in Fig. 3. The SMR is represented with an array of L–C circuits. The Lagrangian $\mathcal{L}$ of the system is expressed in terms of node fluxes ϕ_j,

$$\mathcal{L} = \sum_j\left[\frac{C}{2}\dot{\phi}_j^2 - \frac{1}{2L}(\phi_{j+1} - \phi_j)^2\right] + \frac{C_g(X)}{2}(\dot{\phi}_{j_0} - V_g)^2 \tag{10}$$

where j_0 is the node where the coupling takes place.

Let us start in the case where the mechanical oscillator is at rest at $X = 0$. To describe the SMR, the continuous limit depending on the coordinate z can be used with the lineic capacitance $c = C/\mathrm{d}z$ and the lineic inductance $l = L/\mathrm{d}z$. In terms of the field $\phi(z,t)$, coupled at the position z_0 to the mechanical oscillator, the Lagrangian becomes

$$\mathcal{L} = \int \mathrm{d}z\left[\frac{c}{2}\dot{\phi}^2(z,t) - \frac{1}{2l}\phi'^2(z,t) + \frac{C_g^{(0)}}{2}\left(\dot{\phi}(z,t) - V_g\right)^2\delta(z - z_0)\right] \tag{11}$$

The fundamental mode of the cavity is found with the Euler–Lagrange equation $\frac{\mathrm{d}}{\mathrm{d}t}\frac{\partial \mathcal{L}}{\partial \dot{\phi}} = \frac{\partial \mathcal{L}}{\partial \phi}$,

$$\left[c + C_g^{(0)}\delta(z - z_0)\right]\ddot{\phi}(z,t) = \frac{1}{l}\phi''(z,t) \tag{12}$$

The field is factorized into a spatial and a temporal dependence $\phi(z,t) = f(z)\varphi(t)$, with the spatial function normalized to unity $\int f^2 = 1$. The mode frequency ω_c, satisfying $\ddot{\varphi} = -\omega_c^2\varphi$, and the dispersion relation arise from the Euler–Lagrange equation. In the presence of the coupling capacitance, the bare frequency $\bar{\omega}_c$ is renormalized according to $\omega_c = \bar{\omega}_c\sqrt{c/c_\Sigma}$, where we note the capacitance $c_\Sigma = c + f_0^2 C_g^{(0)}$ and the spatial amplitude at the coupling point $f_0 = f(z_0)$. Using the integration by parts for vanishing boundaries $\int \phi'^2 = -\int \phi\phi''$, the spatial dependence of the Lagrangian can be integrated out. Adding the leading contribution of the displacement, one gets

$$\mathcal{L} = \frac{c_\Sigma}{2}\left(\dot{\varphi}^2 - \omega_c^2\varphi^2\right) - \frac{C_g^{(0)}}{2}V_g(2f_0\dot{\varphi} - V_g) + \frac{C_g^{(1)}}{2}(f_0\dot{\varphi} - V_g)^2 X \tag{13}$$

The charge Q conjugate to the phase φ is

$$Q = \frac{\partial \mathcal{L}}{\partial \dot{\varphi}} = \left(c_\Sigma + f_0^2 C_g^{(1)} X\right)\dot{\varphi} - f_0 V_g\left(C_g^{(0)} + C_g^{(1)} X\right) \tag{14}$$

The Hamiltonian $\mathcal{H} = Q\dot{\varphi} - \mathcal{L}$ is then, at first order in the displacement,

$$\mathcal{H} = \frac{(Q + Q_0)^2}{2c_\Sigma} + \frac{c_\Sigma}{2}\omega_c^2\varphi^2 - \frac{f_0^2 C_g^{(1)}}{2c_\Sigma^2}(Q + Q_0)^2 X + \frac{f_0 V_g C_g^{(1)}}{c_\Sigma}(Q + Q_0)X - \frac{1}{2}V_g^2 C_g^{(1)} X \tag{15}$$

where the charge is shifted by $Q_0 = f_0 V_g C_g^{(0)}$.

The Hamiltonian is now suitable to be quantized, in terms of the mechanical creation and annihilation operators, $a^\dagger$ and a, as well as the cavity operators $b^\dagger$ and b of the fundamental mode

$$Q = \sqrt{c_\Sigma \hbar\omega_c/2}\left(a + a^\dagger\right), \qquad \varphi = i\sqrt{\hbar/2c_\Sigma\omega_c}\left(a - a^\dagger\right) \tag{16}$$

The ladder operators of the SMR also satisfy the canonical commutation rules $[b, b^\dagger] = 1$. The quantities can be expressed in terms of the root mean square voltage of the cavity at the coupling point $V_{\mathrm{rms}} = \sqrt{\hbar\omega_c/2c_\Sigma}\, f_0$. Keeping only the leading contributions of the different terms and adding the Hamiltonian $\hbar\omega_m a^\dagger a$ of the linear mechanical oscillator of frequency ω_m, the Hamiltonian reads

$$\mathcal{H} = \hbar\omega_m a^\dagger a + \hbar\omega_c b^\dagger b - \hbar g_{\mathrm{rp}}\left(a + a^\dagger\right)b^\dagger b + \hbar g\left(a + a^\dagger\right)\left(b + b^\dagger\right) - \hbar\epsilon_m\left(a + a^\dagger\right) + \hbar\epsilon_c\left(b + b^\dagger\right) \tag{17}$$

The Hamiltonian is composed of different terms. The first coupling between the mechanical motion and the photon number is the radiation pressure force between the mechanical oscillator and the cavity. Radiation pressure is the usual coupling term between phonons and photons and is used in sideband cooling. The strength is $\hbar g_{\mathrm{rp}} = C_g^{(1)} V_{\mathrm{rms}}^2 X_{\mathrm{zpf}}$. The second coupling term between the mechanical motion and the photon field is due to the gate voltage: $\hbar g = C_g^{(1)} V_{\mathrm{rms}} V_g X_{\mathrm{zpf}}$. This new coupling is linear and essential to obtain coherent oscillations between phonons and photons. The strength is directly controlled by the gate voltage. Finally, static displacements of the mechanical and the cavity fields arise due to the additional voltage, with strength $\hbar\epsilon_m = C_g^{(1)} V_g^2 X_{\mathrm{zpf}}/2$ and $\hbar\epsilon_c = C_g^{(0)} V_{\mathrm{rms}} V_g$. The displacement can be incorporated in a shift of the ladder operators. If one replaces a by $a + \alpha$ and b by $b + \beta$ and calculates the reals α and β to cancel the linear terms in the Hamiltonian, one obtains

$$\mathcal{H} = \hbar\omega_m a^\dagger a + \hbar(\omega_c - 2\alpha g_{\mathrm{rp}})b^\dagger b - \hbar g_{\mathrm{rp}}\left(a + a^\dagger\right)b^\dagger b + \hbar(g - \beta g_{\mathrm{rp}})\left(a + a^\dagger\right)\left(b + b^\dagger\right) \tag{18}$$

where α and β are defined by $\omega_m\alpha + 2g\beta - g_{\mathrm{rp}}\beta^2 = \epsilon_m$ and $\omega_c\beta + 2g\alpha - 2g_{\mathrm{rp}}\alpha\beta = -\epsilon_c$, that is $\alpha \simeq \epsilon_m/\omega_m$ and $\beta \simeq -\epsilon_c/\omega_c$. In practice the shifts are small and we will neglect their contribution. Moreover the coupling terms remain small compared to the frequencies and a rotating wave approximation can be applied. Finally, the coupling Hamiltonian between the mechanical oscillator and the cavity reads

$$\mathcal{H} = \hbar\omega_m a^\dagger a + \hbar\omega_c b^\dagger b + \hbar g_{\mathrm{rp}}\left(a + a^\dagger\right)b^\dagger b + \hbar g\left(a^\dagger b + a b^\dagger\right) \tag{19}$$

where we are interested in the linear coupling regime $g \gg g_{\mathrm{rp}}$, obtained for $V_g \gg V_{\mathrm{rms}}$.

2.3. Coupling to the environment

The NEMS is a macroscopic object connected to the platform. The phonons leak out and a phonon state decays with a rate $\gamma_m = \omega_m/Q_m$, where Q_m is the quality factor of the NEMS. In the experiments the coupling to the environment is suppressed as much as possible to get a large quality factor. When the external bath is not at very low temperature the NEMS is in a thermal state with a finite number of phonons $n_{\rm th}$. The external circuit being big, it can be supposed in thermal equilibrium without memory effect. The effect of the environment on the NEMS can then be described with the formalism of the quantum master equation developed in the field of quantum optics in the Born–Markov approximation [33]. The coherent evolution of the NEMS is governed by the Hamiltonian $\mathcal{H}$ and the incoherent evolution induced by the environment is obtained from the Lindbladian L. The dynamics of the density matrix ρ_m is governed by the following quantum master equation

$$\dot{\rho}_m(t) = \frac{1}{i\hbar}\big[\mathcal{H}, \rho_m(t)\big] + \mathrm{L}\rho_m(t) \tag{20}$$

where the Lindbladian reads

$$\mathrm{L}_m\rho_m = \frac{\gamma_m}{2}(1-n_{\rm th})\big[2a\rho_m a^\dagger - a^\dagger a\rho_m - \rho_m a^\dagger a\big] + \frac{\gamma_m}{2}n_{\rm th}\big[2a^\dagger\rho_m a - aa^\dagger\rho_m - \rho_m aa^\dagger\big] \tag{21}$$

In the following we will suppose that the temperature is smaller than the frequency of the NEMS so that in the absence of external drive the NEMS is frozen in the ground state. This corresponds to a bath at zero temperature $n_{\rm th} = 0$. An analogous Lindbladian is also obtained for the SMR of damping rate γ_c

$$\mathrm{L}_c\rho_c = \frac{\gamma_c}{2}\big[2b\rho_c b^\dagger - b^\dagger b\rho_c - \rho_c b^\dagger b\big] \tag{22}$$

The two baths are of different nature so the two Lindbladians can be summed up even if the systems are coupled.

2.4. Driving of the NEMS

The NEMS can be directly driven by a piezoelectric on the platform biased by an oscillating voltage. To drive the NEMS in the GHz domain it is more convenient to make use of the Laplace force. When a magnetic field B is applied in the direction perpendicular to the platform and an oscillating current $I = I_0\cos\omega_d t$ flows in the NEMS, the Laplace force acts on the nanobeam and makes it move in the plane of the platform. The amplitude of the force is $I_0\ell B$, where ℓ is the length of the beam, and the corresponding work is $\hbar\epsilon = I_0\ell B X_{\rm zpf}$. The driving Hamiltonian is then $H_d = \hbar\epsilon(a+a^\dagger)\cos\omega_d t$, which can be simplified in the weak driving regime using the rotating approximation,

$$\mathcal{H}_d = \hbar\epsilon\big[a^\dagger \mathrm{e}^{i\omega_d t} + a\mathrm{e}^{-i\omega_d t}\big] \tag{23}$$

When the NEMS is driven from the ground state during a time t, the phonons are in a coherent state of phase $-i\epsilon t$ after a time t. In the presence of dissipation, a steady state is reached with a phase $-2i\epsilon/\gamma_m$ [33].

3. Detection of phonons

3.1. The phonotonic Josephson junction

We consider a NEMS coupled to a qubit and an SMR, as depicted in Fig. 1. The effect of the qubit is kept in the Kerr nonlinearity, and we treat this coupled system as a nonlinear mechanical resonator (NMR). We also focus on the linear coupling regime between the NEMS and the SMR on resonance $\omega_m = \omega_c \equiv \omega_0$ and neglect the radiation pressure term. As discussed in the previous section, the quantum dynamics of the driven and linearly coupled NMR–SMR is obtained from the Hamiltonian

$$\mathcal{H} = \hbar\omega_0\big(a^\dagger a + b^\dagger b\big) + \hbar\kappa a^\dagger a^\dagger aa + \hbar g\big(a^\dagger b + b^\dagger a\big) + \hbar\epsilon\big[a^\dagger \mathrm{e}^{i\omega_d t} + a\mathrm{e}^{-i\omega_d t}\big] \tag{24}$$

and the Lindbladian

$$\mathrm{L}\rho = \frac{\gamma_m}{2}\big[2a\rho a^\dagger - a^\dagger a\rho - \rho a^\dagger a\big] + \frac{\gamma_c}{2}\big[2b\rho b^\dagger - b^\dagger b\rho - \rho b^\dagger b\big] \tag{25}$$

The hybrid Bose Hubbard equation (24) is similar to the Hamiltonian of a Bose Josephson junction, where interacting atoms can tunnel between two wells of a trapping potential [34]. Hamiltonian (24) realizes a “phonotonic Josephson junction”, presented in Fig. 1.

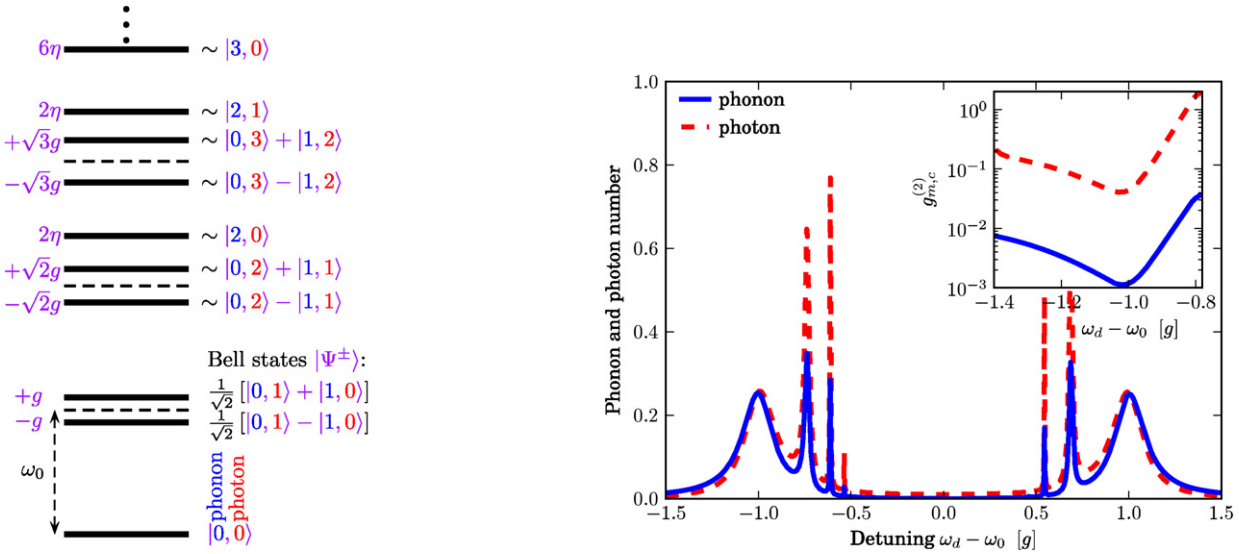

Fig. 4. Left: Schematics of the energy spectrum of the system for $\eta \gg g$. The first excited states are the maximally entangled Bell states $|\Psi^{\pm}\rangle$ and are off resonance with the states with more than one excitation. Right: Spectroscopy of the energy spectrum. Steady state phonon number and photon number as a function of the driving frequency. Inset: Second order correlation functions. Anti-bunching occurs at $\omega_d = \omega_0 \pm g$ where phonon and photon blockade take place. The anharmonicity is $\eta/2\pi = 10$ MHz and the coupling is $g/2\pi = 1$ MHz for quality factors $Q_m = 10^5$ and $Q_c = 10^6$ and the driving amplitude is $\epsilon/2\pi = 0.1$ MHz.

3.2. Detection of phonon blockade with photons

Let us start with an NMR alone, without the SMR. The energy spectrum is composed of the Fock states $|n\rangle$ at the eigenfrequencies $\nu_n = \omega_m n + \kappa n(n-1)$. This spectrum is nonlinear and if the NMR is driven in resonance with the first excited state, it is not possible to climb the ladder since this transition is off-resonant with the other ones, i.e. $\omega_d = \nu_1 - \nu_0 \neq \nu_2 - \nu_1$. Only one phonon is created by the driving, which leaks out after a characteristic time γ_m^{-1}. Another one is then created and so on, so that the phonons go out one by one. In the presence of the effective interaction, the phonons have an anti-bunched statistics. This is the phonon blockade phenomenon, analogous to the photon blockade case measured experimentally in cavity QED [35]. The main problem of the phononic twin is the detection, since the amplitude of motion is so tiny that the quantum signal is lost in the noise. Photon blockade has however been measured recently in a circuit-QED experiment [36] and microwave photons have a huge potential to reveal the behavior of the phonons.

The spectrum of the NMR linearly coupled to the SMR is shown in Fig. 4 in the Fock basis $|n_m, n_c\rangle$, where $n_{m,c}$ is the phonon and photon number respectively. The nth state of the bare linear mechanical oscillator is replaced by $n+1$ states with a total number of excitation $n = n_m + n_c$. The subspaces correspond to the linear span of $\{|k, n-k\rangle;\ 0 \leqslant k \leqslant n\}$. The first excited states are the maximally entangled Bell states

$$\left|\Psi^{\pm}\right\rangle = \tfrac{1}{\sqrt{2}}\left(|0,1\rangle \pm |1,0\rangle\right) \tag{26}$$

with the energy $\hbar\omega_0 \pm \hbar g$. The dependence on the anharmonicity appears for a number of excitations $n \geqslant 2$. For a strong nonlinearity $\eta \gg g$, the spectrum is composed of two entangled states $|0,n\rangle \pm |1,n-1\rangle$ at $\omega_0 \pm \sqrt{n}g$ and $n-1$ factorized states $\{|k,n-k\rangle;\ 2 \leqslant k \leqslant n\}$ located at $\hbar\omega_0 + k(k-1)\hbar\eta$. The nonlinearity of this spectrum allows for excitation blockade. Indeed, because the energy of the states $|\Psi^{\pm}\rangle$ is not resonant with higher states, if the system is excited from the ground state at the frequency $\omega_d = \omega_0 \pm g$, only one excitation is created and symmetrically shared between the NEMS and the SMR. The maximal hybrid entanglement ensures that the phonons and the photons have a pretty close dynamics. The cavity thus constitutes a reliable measurement device to detect the state of the resonator through the photon statistics.

The anti-bunched statistics of the phonon and the photon fields is revealed with the second order correlation function [37]

$$g_m^{(2)} = \frac{\langle a^\dagger a^\dagger a a\rangle}{\langle a^\dagger a\rangle^2} \tag{27}$$

and similarly $g_c^{(2)}$ for the photons, replacing the operators a by b. The second order correlation function measures the population of the states with two or more excitations and vanishes in the blockade regime. Fig. 4 presents the response of the system to the driving current when the driving frequency is tuned. Compared with the dependence of $g_{m,c}^{(2)}$ on ω_d (see the insert), it shows that blockade occurs at $\omega_d - \omega_0 = \pm g$ where the second order correlation function is minimized. Fig. 5, left panel, shows the value of the second order correlation function against the anharmonicity for different coupling

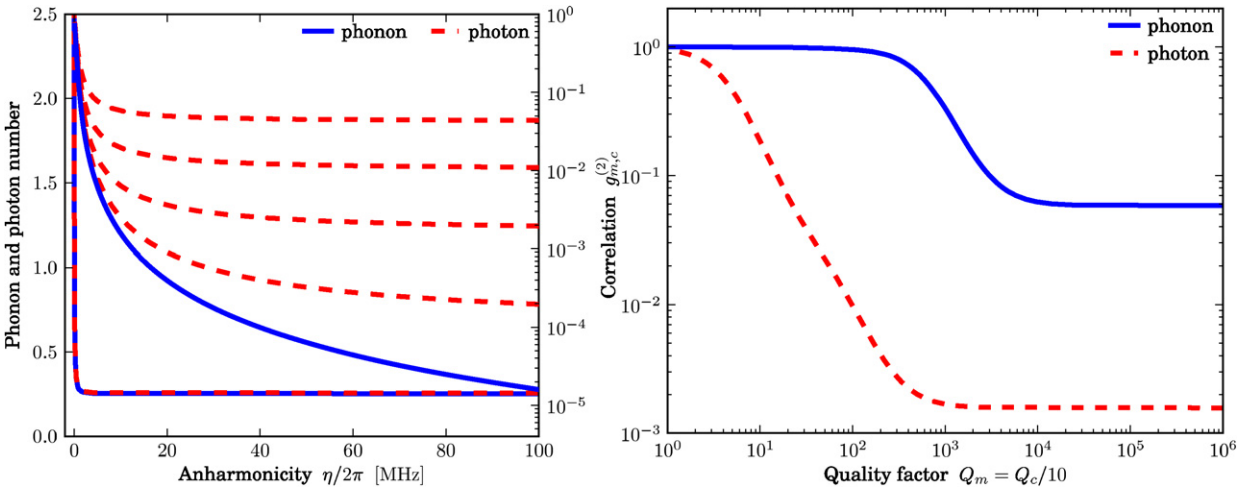

Fig. 5. Left: Steady state phonon and photon numbers (angled lines) and second order correlation functions (smooth lines) as a function of the anharmonicity for different values of the coupling $g/2\pi = 1,\ 2,\ 5,\ 20$ MHz from top to bottom. Right: Second order correlation functions as a function of the quality factors. Both phonon and photon blockade are observed for quality factors $Q_{m,c} \sim 10^3$. The anharmonicity is $\eta/2\pi = 10$ MHz, the coupling is $g/2\pi = 1$ MHz, and the driving amplitude is $\epsilon/2\pi = 0.1$ MHz.

strengths. The transition from photon anti-bunching to photon bunching is observed for small anharmonicities or when, for a fixed anharmonicity, the coupling decreases. Fig. 5, right panel, shows the value of the second order correlation function against the quality factors. Phonon blockade is transduced into photon blockade for quality factors of at least few thousands. For very short lifetimes the coherence is lost and the correlators tend toward unity. The linear coupling thus transfers phonon blockade into photon blockade in a linear SMR, which can then be measured experimentally through the photon statistics.

4. Manipulation of phonons

4.1. Coherent oscillations and self-trapping

We start with a classical description of the phonotonic Josephson junction in the absence of dissipation. The initial state is a coherent state with n phonons obtained from the driving of the NEMS. The driving is then switched off and the system evolves with a fixed number n of particles. To describe the dynamics of the junction, two quantities are useful: the number imbalance $z = \langle a^\dagger a - b^\dagger b\rangle/n$ between the phonons and the photons and the phase difference $\varphi = \arg\langle a^\dagger b\rangle$ between the two resonators. The system is governed by the following set of nonlinear differential equations

$$\dot{z}(\tau) = \sqrt{1 - z^2(\tau)}\sin\varphi(\tau) \tag{28}$$

$$\dot{\varphi}(\tau) = \Lambda\big[1 + z(\tau)\big] - \frac{z(\tau)}{\sqrt{1 - z^2(\tau)}}\cos\varphi(\tau) \tag{29}$$

where the time has been rescaled to $\tau = 2gt$. Eqs. (28), (29) are obtained from the number-phase representation of the time derivatives of $\langle a^\dagger a\rangle$, $\langle b^\dagger b\rangle$, and $\langle a^\dagger b\rangle$. Two regimes arise depending on the parameter $\Lambda = n\eta/2g$ with respect to the critical value $\Lambda_c = 2$ [38]. For large couplings, $\Lambda < \Lambda_c$, coherent oscillations take place between the phonons and photons. For large anharmonicities, $\Lambda > \Lambda_c$, the oscillations are frozen and the particles are self-trapped. The critical value corresponds to a critical coupling $g_c = n\eta/4$. These two regimes are presented in Fig. 6. The time average of the imbalance vanishes in the oscillating regime and tends to unity in the self-trapping regime.

4.2. Manipulation of entanglement with photons

SMRs are powerful not only in the detection but also in the creation of quantum states. An arbitrary quantum state can be synthesized using the right coupling sequence with a qubit [39]. The interplay between coherent oscillations and blockade can then be used to create entangled states between phonons and photons such as the two Bell states

$$|\Psi_\theta\rangle = \tfrac{1}{\sqrt{2}}\big(|1,0\rangle + \mathrm{e}^{i\theta}|0,1\rangle\big) \tag{30}$$

$$|\Phi_\theta\rangle = \tfrac{1}{\sqrt{2}}\big(|0,0\rangle + \mathrm{e}^{i\theta}|1,1\rangle\big) \tag{31}$$

They are maximally entangled and can be obtained from the suitable photonic state. The Bell state $|\Psi_\theta\rangle$ is obtained from the photonic state $|1\rangle_c$ after a time $t_\Psi = \pi/4g$. The Bell state $|\Phi_\theta\rangle$ is obtained from the photonic state $\frac{1}{\sqrt{2}}(|0\rangle_c + |2\rangle_c)$ after

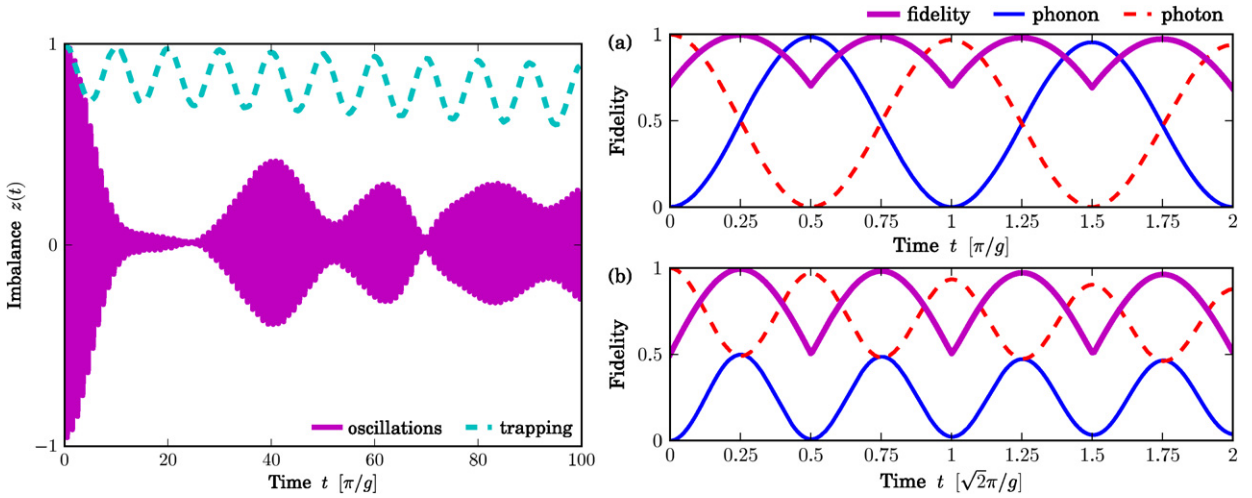

Fig. 6. Left: Time evolution of the number imbalance in the self-trapping regime ($\eta/2\pi = 10$ MHz and $g/2\pi = 1$ MHz) and the oscillating regime ($\eta/2\pi = 1$ MHz and $g/2\pi = 10$ MHz). Quality factors are $Q_m = Q_c = 10^5$. Right: Time evolution of the system for $g/2\pi = 10$ MHz and $\eta/2\pi = 1$ MHz. The initial state is $|0\rangle_m \otimes |1\rangle_c$ in (a) and $|0\rangle_m \otimes \frac{1}{\sqrt{2}}(|0\rangle_c + |2\rangle_c)$ in (b). The fidelity of the Bell state $|\Psi_\theta\rangle$ is plotted in (a) and $|\Phi_\theta\rangle$ in (b). The maximum fidelity is higher than 99%.

a time $t_\Phi = \pi/\sqrt{8}g$. The factor $\sqrt{2}$ comes from the initial state $|2\rangle_c$. The accuracy of the synthesis can be quantified with the fidelity

$$\mathcal{F}_{|\psi\rangle} = \sqrt{\langle\psi|\rho|\psi\rangle} \tag{32}$$

In the case of the Bell states, in the absence of dissipation, the fidelity turns out to be

$$\mathcal{F}_{|\Psi_\theta\rangle}(t) = \sqrt{\tfrac{1}{2}\big(1 + \big|\sin(\pi t/2t_\Psi)\big|\big)} \tag{33}$$

$$\mathcal{F}_{|\Phi_\theta\rangle}(t) = \tfrac{1}{2}\big(1 + \big|\sin(\pi t/2t_\Phi)\big|\big) \tag{34}$$

The fidelity in the presence of dissipation is presented in Fig. 6. We obtain $\mathcal{F}_{|\Psi_\theta\rangle}(t_\Psi) = 99.6\%$ and $\mathcal{F}_{|\Phi_\theta\rangle}(t_\Phi) = 99.3\%$. A direct measurement of the entanglement in this bipartite system in the presence of dissipation is however not possible since it requires information on the full density matrix and only the one of the SMR is accessible experimentally.

5. Conclusion

Coupling NEMS to qubits and SMRs let phonons enter in the field of circuit-QED and interact with Cooper pairs and microwave photons. A rich physics stems from the nascent field of circuit quantum optomechanics. The possibility to couple NEMS to different quantum systems such as spins, cold atoms and optical photons, enables for instance the use of NEMS as quantum transducers. The behavior of massive systems above the Planck mass is also a fundamental test of quantum mechanics for macroscopic systems. It will give insights in the understanding of the transition from the quantum to the classical world and in the interplay between quantum mechanics and gravitation.

Acknowledgements

The authors thank Yaroslav M. Blanter and Stefano Pugnetti for useful discussions. Financial support from EU through the projects QNEMS, NANOCTM and SOLID is gratefully acknowledged.

References

[1] A.N. Cleland, Foundations of Nanomechanics, Springer, 2002.
[2] M. Poot, H.S.J. van der Zant, Phys. Rep. 511 (2012) 273.
[3] A.J. Leggett, Progr. Theoret. Phys. Suppl. 69 (1980) 80;
See also A.J. Leggett, J. Phys.: Condens. Matter 14 (2002) R415.
[4] I. Wilson-Rae, N. Nooshi, W. Zwerger, T.J. Kippenberg, Phys. Rev. Lett. 99 (2007) 093901;
F. Marquardt, J.P. Chen, A.A. Clerk, S.M. Girvin, Phys. Rev. Lett. 99 (2007) 093902.
[5] S. Gröblacher, J.B. Hertzberg, M.R. Vanner, G.D. Cole, S. Gigan, K.C. Schwab, M. Aspelmeyer, Nature Phys. 5 (2009) 485;
Y.-S. Park, H. Wang, Nature Phys. 5 (2009) 489;
A. Schliesser, O. Arcizet, R. Rivière, G. Anetsberger, T.J. Kippenberg, Nature Phys. 5 (2009) 509;
Q. Lin, J. Rosenberg, X. Jiang, K.J. Vahala, O. Painter, Phys. Rev. Lett. 103 (2009) 103601;

T. Rocheleau, T. Ndukum, C. Macklin, J.B. Hertzberg, A.A. Clerk, K.C. Schwab, Nature 463 (2010) 72;
J.D. Teufel, D. Li, M.S. Allman, K. Cicak, A.J. Sirois, J.D. Whittaker, R.W. Simmonds, Nature 471 (2011) 204.
[6] A.D. O'Connell, M. Hofheinz, M. Ansmann, R.C. Bialczak, M. Lenander, E. Lucero, M. Neeley, D. Sank, H. Wang, M. Weides, J. Wenner, J.M. Martinis, A.N. Cleland, Nature 464 (2010) 697.
[7] J.D. Teufel, D. Li, M.S. Allman, K. Cicak, A.J. Sirois, J.D. Whittaker, R.W. Simmonds, Nature 471 (2011) 204.
[8] J. Chan, T.P. Mayer Alegre, A.H. Safavi-Naeini, J.T. Hill, A. Krause, S. Gröblacher, M. Aspelmeyer, O. Painter, Nature 478 (2011) 89.
[9] A.N. Cleland, M.R. Geller, Phys. Rev. Lett. 93 (2004) 070501.
[10] M.R. Geller, A.N. Cleland, Phys. Rev. A 71 (2005) 032311.
[11] E.J. Pritchett, M.R. Geller, Phys. Rev. A 72 (2005) 010301(R).
[12] X. Zou, W. Mathis, Phys. Lett. A 324 (2004) 484.
[13] J. Clarke, F.K. Wilhelm, Nature 453 (2008) 1031.
[14] A.D. Armour, M.P. Blencowe, K.C. Schwab, Phys. Rev. Lett. 88 (2002) 148301.
[15] I. Martin, A. Shnirman, L. Tian, P. Zoller, Phys. Rev. B 69 (2004) 125339.
[16] P. Rabl, A. Shnirman, P. Zoller, Phys. Rev. B 70 (2004) 205304.
[17] L.F. Wei, Y.-X. Liu, C.P. Sun, F. Nori, Phys. Rev. Lett. 97 (2006) 237201.
[18] A.D. Armour, M.P. Blencowe, New J. Phys. 10 (2008) 095004.
[19] J. Hauss, A. Fedorov, S. André, V. Brosco, C. Hutter, R. Kothari, S. Yeshwanth, A. Shnirman, G. Schön, New J. Phys. 10 (2008) 095018.
[20] B.R. Trees, Y.H. Helal, J.S. Schiffrin, B.M. Siller, Phys. Rev. B 76 (2007) 224513;
J. Wabnig, J. Rammer, A.L. Shelankov, Phys. Rev. B 75 (2007) 205319.
[21] J. Wabnig, J. Rammer, A.L. Shelankov, Phys. Rev. B 75 (2007) 205319.
[22] M.D. LaHaye, J. Suh, P.M. Echternach, K.C. Schwab, M.L. Roukes, Nature 459 (2009) 960.
[23] X. Zhou, A. Mizel, Phys. Rev. Lett. 97 (2006) 267201.
[24] E. Buks, M.P. Blencowe, Phys. Rev. B 74 (2006) 174504.
[25] F. Xue, Y.D. Wang, C.P. Sun, H. Okamoto, H. Yamaguchi, K. Semba, New J. Phys. 9 (2007) 35.
[26] Y.D. Wang, K. Semba, H. Yamaguchi, New J. Phys. 10 (2008) 043015.
[27] J. Zhang, Y.-X. Liu, F. Nori, Phys. Rev. A 79 (2009) 052102.
[28] S. Etaki, M. Poot, I. Mahboob, K. Onomitsu, H. Yamaguchi, H.S.J. van der Zant, Nature Phys. 4 (2008) 785.
[29] A. Wallraff, D.I. Schuster, A. Blais, L. Frunzio, R.-S. Huang, J. Majer, S. Kumar, S.M. Girvin, R.J. Schoelkopf, Nature 431 (2004) 162.
[30] N. Didier, S. Pugnetti, Y.M. Blanter, R. Fazio, Detecting phonon blockade with photons, Phys. Rev. B 84 (2011) 054503.
[31] N. Didier, S. Pugnetti, Y.M. Blanter, R. Fazio, arXiv:1201.6293, 2012.
[32] G.-L. Ingold, Yu.V. Nazarov, Single charge tunneling, in: H. Grabert, M.H. Devoret (Eds.), NATO ASI Series B, vol. 294, Plenum, 1992.
[33] M.O. Scully, M.S. Zubairy, Quantum Optics, Cambridge University Press, 1997;
H.J. Carmichael, Statistical Methods in Quantum Optics, vol. 1, Springer, 1998;
D.F. Walls, G.J. Milburn, Quantum Optics, 2nd edition, Springer, 2008.
[34] M. Albiez, R. Gati, J. Fölling, S. Hunsmann, M. Cristiani, M.K. Oberthaler, Phys. Rev. Lett. 95 (2005) 010402;
G. Ferrini, A. Minguzzi, F.W.J. Hekking, Phys. Rev. A 78 (2008) 023606;
D.V. Averin, T. Bergeman, P.R. Hosur, C. Bruder, Phys. Rev. A 78 (2008) 031601(R).
[35] K. Hammerer, M. Wallquist, C. Genes, M. Ludwig, F. Marquardt, P. Treutlein, P. Zoller, J. Ye, H.J. Kimble, Phys. Rev. Lett. 103 (2009) 063005.
[36] C. Lang, D. Bozyigit, C. Eichler, L. Steffen, J.M. Fink, A.A. Abdumalikov, M. Baur, S. Filipp, M.P. da Silva, A. Blais, A. Wallraff, Phys. Rev. Lett. 106 (2011) 243601.
[37] L. Mandel, E. Wolf, Optical Coherence and Quantum Optics, Cambridge University Press, 1995.
[38] A. Smerzi, S. Fantoni, S. Giovanazzi, S.R. Shenoy, Phys. Rev. Lett. 79 (1997) 4950.
[39] M. Hofheinz, H. Wang, M. Ansmann, R.C. Bialczak, E. Lucero, M. Neeley, A.D. O'Connell, D. Sank, J. Wenner, J.M. Martinis, A.N. Cleland, Nature 459 (2009) 546.